九州大学学術情報リポジトリ
Kyushu University Institutional Repository

Numerical Investigation of the Properties of Japanese Historical Brick Masonry Structures

Chhabi Mishra
Structural Engineer, Hulas Steel Industries Pvt. Ltd.

Yamaguchi, Kentaro
Faculty of Human-Environment Studies, Kyushu University : Professor

https://doi.org/10.5109/7323394

出版情報：Proceedings of International Exchange and Innovation Conference on Engineering & Sciences (IEICES). 10, pp.1091-1099, 2024-10-17. International Exchange and Innovation Conference on Engineering & Sciences
バージョン：
権利関係：Creative Commons Attribution-NonCommercial-NoDerivatives 4.0 International

KYUSHU UNIVERSITY

Numerical Investigation of the Properties of Japanese Historical Brick Masonry Structures

Chhabi Mishra[1], Kentaro Yamaguchi[2]
[1]Structural Engineer, Hulas Steel Industries Pvt. Ltd.;
[2]Professor, Faculty of Human-Environment Studies, Kyushu University
chhabi.mishra7@gmail.com; yamaguchi@arch.kyushu-u.ac.jp

Abstract: *The purpose of this study was to discretize a numerical model that can be used to assess the behavior of brick masonry with cement mortar. The behavior of unreinforced brick masonry (URM) was investigated through numerical simulation. A homogenous macro model was used in ABAQUS software to reproduce a previously performed diagonal compression test and horizontal loading test of a wall built of brick masonry with cement mortar. Material properties such as density, E, and Poisson's ratio were input to the software. The objective of this study was to confirm Young's modulus and Poisson's ratio so that it can used in macro modeling. To confirm Young's modulus and Poisson's ratio the numerical modeling of diagonal compression test and horizontal loading test were conducted. The Poisson's ratio obtained from transducers gave closer analytical results to experimental results compared to Poisson's ratio obtained from Rosette's strain gauge. From the numerical analysis of diagonal compression model and from contours in the model, it was observed that most of the compressive forces pass through the centre of the specimen and are only concentrated in the area directly under the load rather than distributing to the whole cross-sectional area of the specimen. The highest value of the modulus of elasticity (E = 6870 MPa) was obtained for samples loaded perpendicularly to horizontal joints (θ_{strut}=90°). For the horizontal loading test, the value of E = 5700 MPa was obtained from the analysis (θstrut = 67.43°). The values of shear modulus G (calculated from the diagonal transducers in diagonal compression test) are within the range of 8–17% of the value of modulus of elasticity E (prism compression test) for Nepalese and Japanese historical brick masonry.*

Keywords: Historical brick masonry, Numerical modeling, Diagonal compression model, Horizontal loading model, Rosette's Poisson's ratio

1. INTRODUCTION

Brick masonry is one of the earliest and most widely utilized types of construction in the world. Depending on their geometric configurations, arrangement, and mechanical properties, brick units and mortar combine to construct various masonry walls (Ma et al., 2022; Abdulla et al., 2017). Moderate to strong earthquakes resulted in partial damage or complete collapse of the Unreinforced reinforced masonry (URM) structures due to cracking, resulting in significant financial losses and a high death toll (Penna et al., 2014; Kouris and Triantafillou, 2018).

URM structures are load-bearing type structures and their compressive capacity is noticeably greater than that of tension, shear, and bending. Under external forces such as earthquakes, and wind load, URM structures are susceptible to macro fractures, which lead to successive failure and damage. URM walls frequently exhibit horizontal, vertical, and diagonal cracks when subjected to seismic action (Sun et al., 2009).

For experimental research on the seismic performance of masonry walls, numerical simulations offer a workable substitute approach that can mimic both the linear and nonlinear behaviors of masonry (Mojsilović et al., 2013; Roca et al., 2010). Furthermore, numerical simulation can employ either macro modeling techniques which are typically used to simulate structural performance, or micro modeling techniques, which are based on the needed degree of accuracy and model size (Holler et al., 2004; Hu et al., 2023). Based on the findings of experiments, the material properties are required for the accuracy and dependability of the numerical model. It is feasible to alter the intended parameters and confirm the impact of each component after the model has been calibrated (Oliveira, 2014).

Various methods have been developed for analyzing the behavior of masonry structures. Lourenço stated that the modeling techniques fall into three main categories: macro-modeling, simplified micro-modeling, and detailed micro-modeling (Lourenco, 1998). The simulation of units, mortar, and the unit-mortar interface are all included in micro-modeling. It works well for examining the structural behavior of small masonry components, but it takes a lot of CPU time for models with a large number of elements (Annecchiarico et al., 2010). However, the macro-modeling approach requires less computing power and is the preferred method in use today. Masonry is considered a continuous material and there is no differentiation between units and joints in the macro-modeling approach. The masonry was considered an isotropic, homogeneous continuum in this approach. Units and mortar in the joints were taken into consideration in the case of the simplified micro-modeling approach, but no interface element was taken into consideration (Annecchiarico et al., 2010).

This study used a macro model that is simple to use for seismic analysis and structural design. This work aimed to explore a numerical technique for the analysis of the behavior of brick masonry walls in the elastic range. Furthermore, through numerical simulation, the behavior of brick masonry walls for diagonal compression test and horizontal loading test for Japanese historical brick masonry was also examined through a macro modeling approach. This study also gives insight into the structural behavior of historical brick masonry subjected to horizontal loading. This study also confirms Young's modulus and Poisson's ratio of Japanese historical masonry so that it can be used in macro modeling analysis.

2. MATERIALS AND METHODS

2.1 Description of the Experiment

Uniaxial compression experiments were conducted to clarify the basic mechanical properties of elements of brick walls (unit bricks, mud mortar, and masonry prisms). From the three specimens of the masonry prism, average compressive strength and Young's modulus E for Japanese masonry were determined. From the diagonal compression experiment, the shear strength and shear modulus G were determined. Also, a horizontal loading test was done to determine the load-displacement characteristics and stiffness of the Japanese wall.
For the diagonal compression experiment load was applied and displacement transducers measured the compressive shortening and tensile elongation of the specimen. Horizontal loading tests were carried out on an inverted T-shaped specimen where a pre-compressive load of 0.21 N/mm^2 was applied and horizontal loads were applied in positive and negative directions to the wall. Displacement transducers were set up to measure the shear deformation, bending deformation, and horizontal displacement. Figure 1a) shows the prism compression test setup. Figure 1b) shows the diagonal compression test setup and 1c) shows a schematic diagram of the loading of the diagonal compression test. Figure 2a) shows the horizontal loading test setup and Figure 2b) shows the position of transducers on the specimen. Figure 3a) shows the diagonal compression test specimen showing the transducer's position and Figure 3b) shows the diagonal compression test specimen showing Rosette's strain gauges.

a)

b)

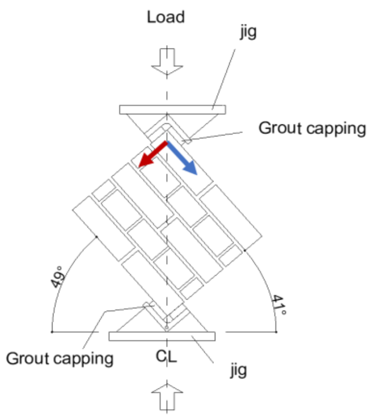

c)

Figure 1: a) Prism compression test b) diagonal compression test c) schematic diagram of loading of diagonal compression test

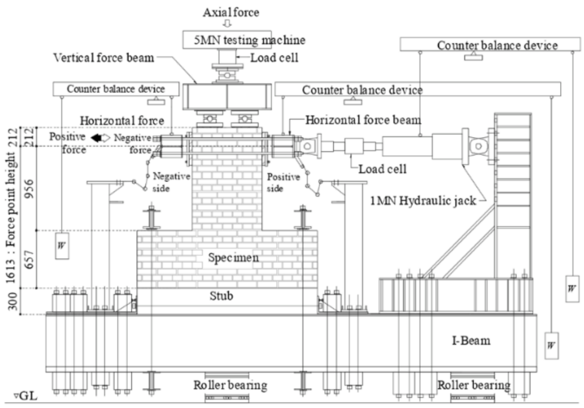

a)

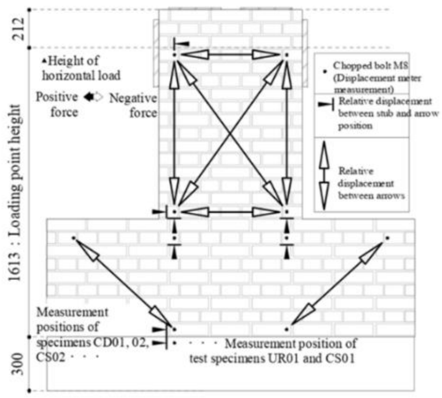

b)

Fig. 2: a) Horizontal loading test setup b) Position of transducers on the specimen

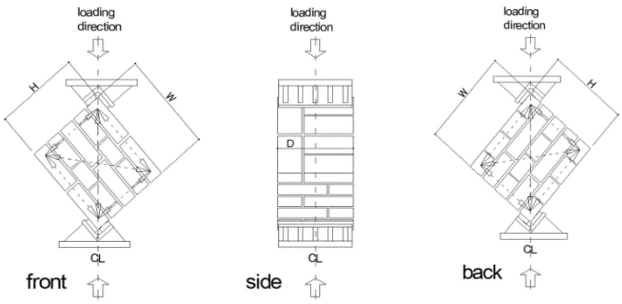

a)

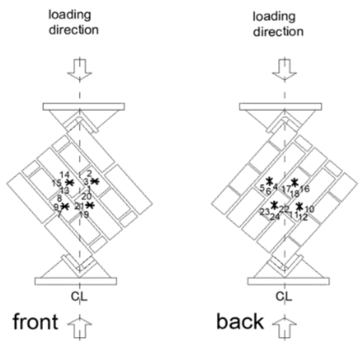

b)

Figure 3: a) Diagonal compression test specimen showing transducers position

b) Diagonal compression test specimen showing Rosette strain gauges

2.2 Research Methodology

A case study on the results obtained in various experiments of brick masonry that constitutes Japanese historical buildings was conducted. Firstly, the mechanical properties from the experimental results were determined. Secondly, for numerical modeling, load-deformation relationships from experimental results were also confirmed. From the Diagonal compression test, the shortening and elongation of diagonal transducers before crack propagation were noted. For the horizontal loading test, the first crack point observed was at approximately 75% of the maximum load. The first crack point was identified from experimental data by using hysteresis and envelope curves. Shear deformation from diagonal transducers, bending deformation from vertical transducers, and horizontal displacement before the crack point were also noted. Thirdly, numerical analysis was performed on the diagonal compression model and horizontal loading test models. This stage was articulated in two steps, which included (i) validation of the diagonal compression model to confirm Poisson's ratio, and (ii) validation of the horizontal loading test model. The numerical models were developed and validated using a macro model elastic analysis. The analysis was conducted using the general-purpose finite element method software, ABAQUS. Since applying the micro model to historical buildings is more difficult and time-consuming, the goal of this research is to create an analysis technique that uses macro modeling to more accurately depict the behavior of real structures. Furthermore, when designing structures using brittle masonry, it is not practical to create huge deformations. For this reason, the majority of this work concentrates on minor deformation regions that can be utilized to create safer structural designs.

The discretization of a numerical model for evaluating brick masonry behavior was the aim of this study. Numerical simulation was used to study the behavior of Japanese URM walls. The material properties for macro modeling in any FEM software are Young's modulus of elasticity and Poisson's ratio which are important parameters for macro modeling in the elastic range. Masonry is heterogeneous and anisotropic in nature due to brick units and mortar. However, in macro modeling masonry is considered isotropic and homogenous where the software automatically calculates shear modulus (G) from the values of Young's modulus (E) and Poisson's ratio (v). For the confirmation of value of Poisson's ratio for macro modeling, a numerical analysis of the diagonal compression model was carried out. After confirming the value of v, the numerical analysis on the horizontal loading test model was carried out to confirm the value of Young's modulus (E) in the elastic range.

2.3 Results and Discussion

2.3.1 Determination of Poisson's ratio (from transducers)

Poisson's ratio was calculated as the ratio of strain in the tensile direction to the compressive direction as the difference in tensile and compressive strain was large in the diagonal experiment. Tensile strain is the elongation in the tensile diagonal direction measured by a horizontal displacement transducer. Similarly, compressive strain is the shortening in the compressive diagonal direction measured by the vertical displacement transducer. Poisson's ratio was calculated by taking linear regression of data up to 33% of maximum load (Figure 8.4). The Poisson's ratio of DUR 501, DUR 502, and DUR 503 specimens were 0.0348, 0.0535, and 0.0584, respectively. The average Poisson's ratio was 0.0489

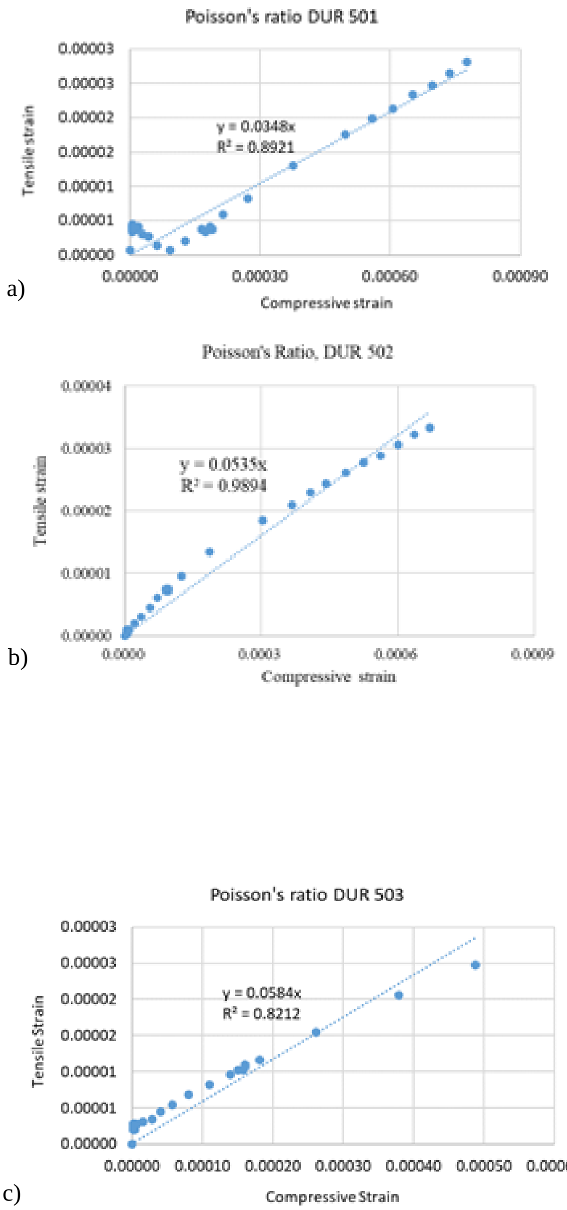

a)

b)

c)

Fig. 4: Poisson's ratio determined by diagonal transducers for a) DUR 501, b) DUR 502, and c) DUR 503 specimens

2.3.2 Determination of Poisson's ratio by Rosette method (from strain gauges)

The principal compressive strain was calculated by equation (1). The principal tensile strain was calculated by equation (2) and shear strain was calculated by equation (3). Where, ε1 is the strain in the horizontal direction, ε2 is the strain in the vertical direction, and ε3 is the strain in the diagonal direction of the Rosette strain gauge. The Poisson's ratio was calculated from the Rosette method as a ratio of tensile strain to compressive strain. The Poisson's ratio was calculated by linear regression of data up to 33% of maximum load as shown in Figure 5. The average Poisson's ratio was determined from all three specimens which was 0.312.

$$\varepsilon_{min} = \frac{1}{2}\left[\varepsilon_1 + \varepsilon_2 - \sqrt{2\{(\varepsilon_1 - \varepsilon_3)^2 + (\varepsilon_2 - \varepsilon_3)^2\}}\right] \quad (1)$$

$$\varepsilon_{max} = \frac{1}{2}\left[\varepsilon_1 + \varepsilon_2 + \sqrt{2\{(\varepsilon_1 - \varepsilon_3)^2 + (\varepsilon_2 - \varepsilon_3)^2\}}\right] \quad (2)$$

$$\gamma_{max} = \sqrt{2\{(\varepsilon_1 - \varepsilon_3)^2 + (\varepsilon_2 - \varepsilon_3)^2\}} \quad (3)$$

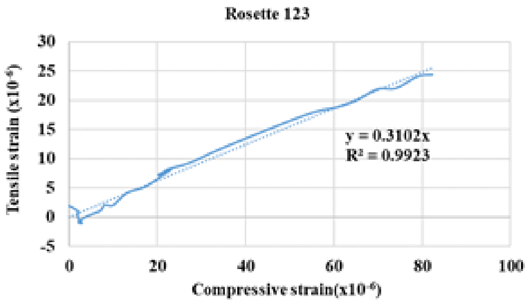

a)

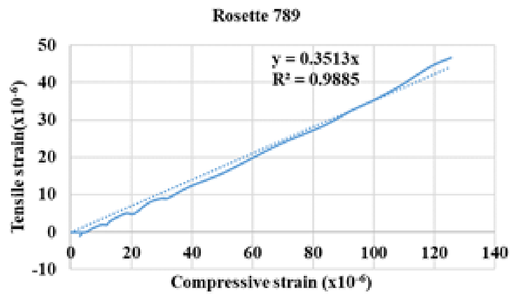

b)

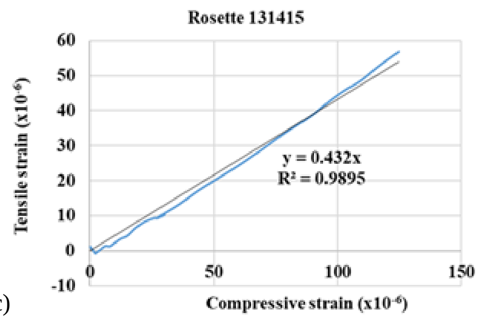

c)

Fig. 5: Poisson's ratio by Rosette method for a) DUR 501, b) DUR 502, and c) DUR 503 specimens

2.3.3 Material properties from prism compression test

The dimensions of masonry prisms are shown in Table 1. Table 2 shows the results of prism compression test. The compressive strength of the brick was 19.2 N/mm^2 (Mishra et al., 2020; Mishra et al., 2021).

Table 1: Dimensions of masonry prism and its component properties

Specimen	Height H	Width W	Depth D	Mortar: Compressive Strength (N/mm^2)	Mortar: Young's Modulus (N/mm^2)
PPC 101	690.3	345.0	464.8		2.42x10^4
PPC 102	689.3	345.5	464.5	29.0	2.43x10^4
PPC 103	689.5	345.0	464.8		2.42x10^4

Table 2: Results from prism compression test

Experiment	Prism average compressive strength (MPa)	Average Young's modulus of masonry prism (MPa)	Density of brick (Kg/m^3)
Prism compression test	15.8	6870	1566

2.3.4 Material properties of diagonal compression test

The size of diagonal compression test specimen is shown in Table 3. The results from diagonal compression test are shown in Table 4. The average shear strength of wall was 0.95 MPa, the average shear modulus (G) was 553 MPa, the average Poisson's ratio (v) was 0.0489, and Young's modulus of elasticity from the equation E = 2(1+V) *G was 1160.083, respectively.

Table 3: Size of the specimens

Specimens		Height H [mm]	Width [mm]	Depth D [mm]
	501	357	410	331
DUR	502	355	410	331
	503	355	410	332

Table 4: Results from diagonal compression test

Exp. Results	Shear strength of wall (MPa)	Shear Modulus G (MPa)	Poisson's ratio from transducers, v	Poisson's ratio from Rosette method, v	E = 2(1+V) xG
Diagonal Compression	0.95	553	0.0489	0.312	1160

2.3.5 Determination of shear modulus by considering the shear deformation due to compressive diagonal and tension diagonal transducers

Shear modulus (G) was calculated as the ratio of shear stress and shear deformation angle. For the calculation of shear deformation angle, the average deformation of compressive and tensile diagonals was considered. However, the shear deformation calculated from shortening of compressive diagonal and elongation in tensile diagonal have large variations in values. Therefore, shear modulus due to compressive diagonal (Gc) and shear modulus due to tensile diagonal (Gt) were calculated separately. The shear modulus was calculated by taking the linear regression of experimental data up to 33% as shown in Figure 6.

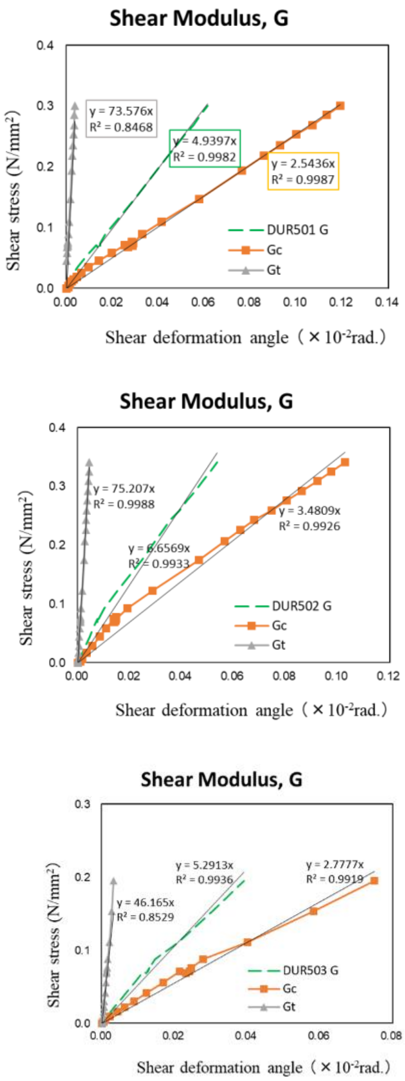

Fig. 6: Shear modulus determination for a) DUR 501, b) DUR 502, and c) DUR 503 specimens

Table 5 shows the results of shear modulus, shear modulus considering only compressive diagonal, and shear modulus considering only the tensile diagonal.

Table 5: Results of shear modulus for URM specimens

Specimens		(G) [N/mm²]	(Gc) [N/mm²]	(Gt) [N/mm²]
	501	493.9	254.3	7358
DUR	502	635.9	348.0	7521
	503	529.1	277.7	4617
Average		553.0	293.4	6498

Where G is shear modulus, Gc is shear modulus considering only the compressive diagonal, Gt is shear modulus considering only the tensile diagonal

2.4 Numerical Modeling of Unreinforced Masonry Walls

A numerical model of a URM wall was created using a three-dimensional solid (or continuum) element in ABAQUS finite element software. C3D8R is a hexahedral 8-node linear brick element with reduced integration. The integration point of the C3D8R element is located in the middle of the element. C3D8R was selected for mesh generation as it is cost-effective and has enhanced convergence compared to full integration (Dauda et al., 2021). A mesh size of 30 mm was used. Masonry was modeled as an isotropic and homogeneous material. Elastic modulus (E) from the prism compression experiment was taken as the E initial for the first iteration.

Using a three-dimensional solid (or continuum) element in ABAQUS finite element software, a numerical model of a URM wall was produced. The element C3D8R is a reduced integration linear brick element with hexahedral eight nodes. The center of the C3D8R element is where its integration point is situated. Because it is more affordable and has better convergence than full integration, C3D8R was chosen for mesh generation (Dauda et al., 2021). A 30 mm mesh size was employed. Masonry was represented as a homogenous, isotropic material. Poisson's ratio and density were also taken as input to the software. For the first iteration, elastic modulus (E), obtained from the prism compression experiment, was used as the initial E. The trials for different values of E during modeling were done until the numerical result was in good agreement with the experimental value.

2.4.1 Numerical Modeling of Diagonal Compression Model

There were two boundary conditions, the bottom base was fixed in the y-direction and the center of base was pinned in the modeling to replicate the experimental condition of the diagonal compression test (Figure 7). The load was applied from the top which was uniformly distributed all over the loading shoe.

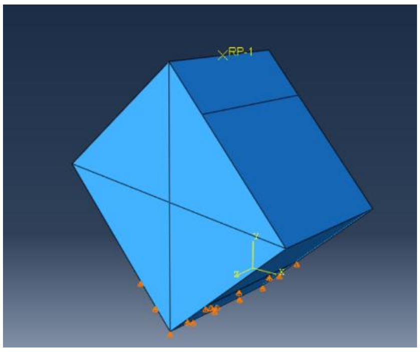

Fig. 7: 3D Abaqus model of diagonal compression test

Table 6 shows the results of numerical analysis of diagonal compression model. Three cases were considered in this study. For case 1, results from the diagonal compression test were taken (G and v) and E was calculated from the equation E = 2(1+V) G. In this case, the v was calculated from transducers. The values v and E were used as input to software during numerical analysis.

For case 2, the same value of E as that of case one was taken and v calculated from the Rosette`s strain gauge was used as input to software during numerical analysis.

For case 3, E was calculated from the equation E = 2(1+V) G by taking v from the Rosette`s strain gauge was used as input to software during numerical analysis.

In this study, Case one gives the least error for both compressive shortening and tensile elongation. However, for tensile elongation, the error % was irrelevant as the tensile elongation was much less compared to compressive shortening.

Table 6: Results of numerical analysis of diagonal compression test

Number of cases	E (N/mm^2)	v	Experimental Results: Compressive shortening (mm)	Experimental Results: Tensile elongation (mm)	Analysis results from Abaqus: Compressive shortening (mm)	% Increase or decrease	Tensile elongation (mm)	% Increase or decrease
Case 1	1160	0.0489			0.232	-11.0	0.035	327.0
Case 2	1160	0.3126	0.2616	0.0082	0.219	-16.0	0.081	888.0
Case 3	1452	0.3126			0.173	-34.0	0.064	680.0

Figure 8a) shows the displacement contour in a vertical direction and Figure 8b) shows the displacement contour in a horizontal direction. Figure 9a) shows the principal compressive strain and Figure 9b) shows the principal tensile strain. The contours show that the part under load was in compression, and the part perpendicular to the load was in tension, which was in good agreement with the experimental results.

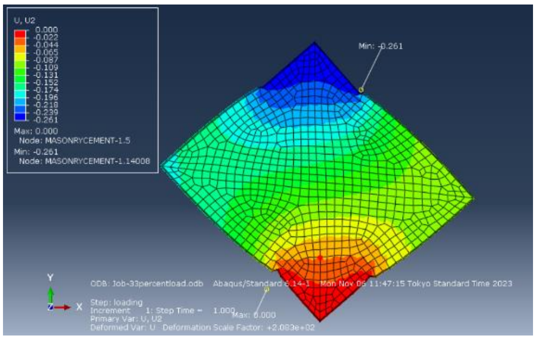

a)

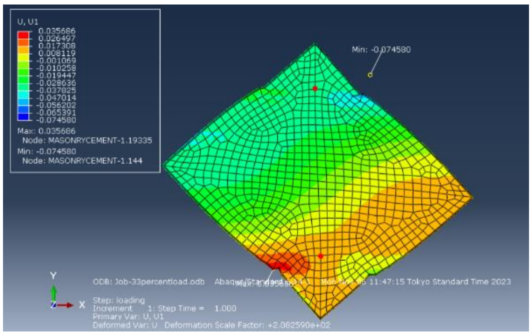

b)

Fig. 8: Displacement contour in a) vertical direction b) horizontal direction

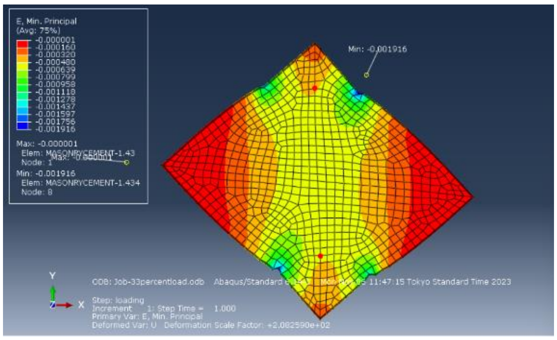

a)

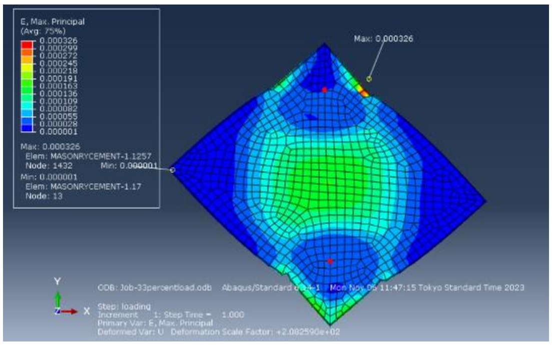

b)

Fig. 9: a) Principal compressive strain b) Principal tensile strain

2.4.2 Selection of best-fit value of Poisson's ratio from numerical modeling of diagonal compression test

The Poisson's ratio obtained from transducers gave closer results compared to Poisson's ratio obtained from Rosette's strain gauge. This might be due to the Rossette's strain gauge being only attached to brick whereas the transducers included the deformation of bricks and mortar together.

From the stress contour in numerical analysis (Figure 9a) and b)), it is clear that the compressive strut is formed under the loading shoe (169 mm) and the effective area for compression is load shoe length times the specimen depth (A=55939 mm2).

Also, from the relation of σ = E*εc where E is the young's modulus of elasticity (1160.083 N/mm2) and εc is the compressive strain from the experimental results, the effective area in the specimen was determined as 59977 mm2. Most of the compressive forces pass through the center of the specimen and are only concentrated in the area directly under the load rather than distributed to the whole cross-sectional area of the specimen. The tensile force also concentrates on a small area rather than distributing to the whole cross-sectional area. This might be the reason for the higher % error for tensile elongation.

The ratio of load shoe length to the total diagonal length multiplied by tensile elongation obtained from analysis gives the actual tensile elongation. This ratio of actual tensile elongation to the compressive shorting obtained from analysis was Poisson's ratio which was close to the value of Poisson's ratio obtained from transducers. Therefore, we selected Poisson's ratio obtained from transducers for further analysis.

2.4.3 Horizontal loading test

Figure 2a) shows the loading arrangement of horizontal load test and Figure 2b) shows the positions of transducers to measure the shear and bending deformation. From the load-displacement behavior, the hysteresis or all loading cycles were plotted. The envelope curve of URM wall was developed from the hysteresis curve. From experimental data and envelope curve, the first crack point was determined and the corresponding displacement was also determined. The first crack point was at approximately 75% of the maximum load as shown in Figure 10. The load-displacement behavior of the horizontal wall test is shown in Table 7. The stiffness was 147.87 KN/mm. At the first crack point, the shear deformation and bending deformation were noted from experimental data.

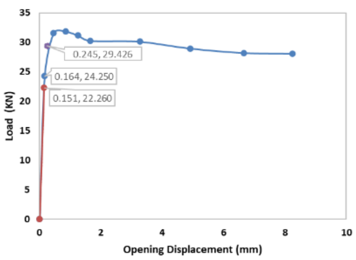

Fig. 8.10: Envelope curve obtained from hysteresis curve of horizontal wall test

Table 7: Load displacement behavior of horizontal wall test

Crack load, H (KN)	Displacement, d (mm)	Stiffness, K=H/d (KN/mm)
24.25	0.164	147.87

2.4.4 Numerical modeling of horizontal loading test

There were three boundary conditions. First was half of the bottom of the RC base fixed in the y-direction, the second was the plate fixed on the RC stub base side which was fixed in the x-direction and third was the spandrel restrained in the y-direction on the left side of the opening wall (Figure 11). The pre-compression load of 0.21 N/mm2 was applied as a uniformly distributed load. The horizontal load was applied from the left side of the specimen and the model was run. From the analysis results, the deformation in compressive diagonal and tensile diagonal were also verified with the experimental results. Similarly, the left vertical and right vertical transducers were also verified with the experimental results. Finally, the top horizontal displacement was also verified with the horizontal loading test experimental data.

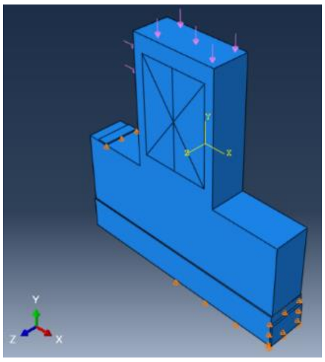

Fig. 11: 3D Abaqus model of horizontal loading test

Table 8 shows the results of numerical analysis of the horizontal loading test for shear deformation and Table 9 shows the results of horizontal loading test for bending deformation. Three cases were studied. Table 8 and 9 show that when the value of E from the diagonal compression test was input to the software, the results deviated far away from the experimental results. When Young's modulus from prism compression test E=6870 N/mm^2 was taken as input to the software along with previously calibrated Poisson's ratio, v, the results were closer to the shear deformation (Table 8). However, the bending deformation % error was higher (Table 9). When Young's modulus of E = 5700 N/mm2 (from trial and error) was taken as input to the software along with previously calibrated Poisson's ratio (v), the numerical results were closer to the experimental values of shear and bending deformation (Table 8 and 9).

Table 8: Results of numerical analysis of horizontal loading test for shear deformation

E (N/mm²)	v	Experimental results (Shear deformation)		Analysis results from Abaqus			
		Compressive shortening (mm)	Tensile elongation (mm)	Compressive shortening (mm)	% Increase or decrease	Tensile elongation (mm)	% Increase or decrease
1160				0.17	541.5	0.14	500.9
6870	0.0489	0.0265	0.0233	0.0277	4.5	0.0233	0.0
5700				0.0329	24.2	0.028	20.2

Table 9: Results of numerical analysis of horizontal loading test for bending deformation

E (N/mm²)	v	Experimental Results (Bending deformation)		Analysis results from Abaqus			
		Left vertical elongation (mm)	Right vertical shortening (mm)	Left vertical elongation (mm)	% Increase or decrease	Right vertical shortening (mm)	% Increase or decrease
1160				0.165	368.0	0.158	348.2
6870	0.0489	0.0353	0.0353	0.028	-20.6	0.0270	-23.4
5700				0.033	-6.4	0.0320	-9.2

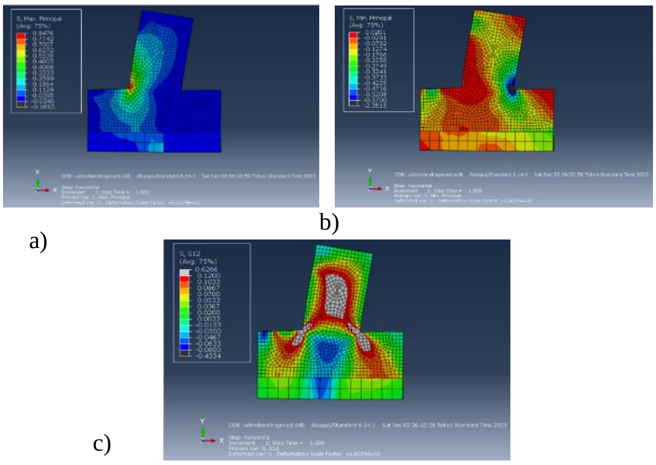

a) b) c)

Fig. 12 a) shows principal tensile stress b) shows principal compressive stress and c) shear stress (xy) for the horizontal loading test model.

2.4.5 Changes in Young's modulus with the angle of the compressive strut with bed joint (θstrut)

The highest value of the modulus of elasticity (E = 6870 MPa) was obtained for samples loaded perpendicularly to horizontal joints (θstrut = 90°). For the horizontal loading test, the value of E = 5700 MPa was obtained from the analysis (θstrut = 67.13°). The lowest value of E = 1160 MPa was obtained for the samples with angle θstrut = 41° (Table 8.10). The lowest value of the coefficient E_θ/E_{90} has been obtained for samples with joints rotated at an angle θ = 49° for the diagonal compression test. Nowak et al. (2021) and Mishra et al. (2023) reported similar results. It has been noted that depending on the angle of the compressive stress trajectory, the anisotropy of the brickwork greatly affects the wall's ability to support loads (Nowak et al., 2021). The analysis made it possible to calculate the masonry strength when the load was applied at various angles to the bed joints.

Table 10: Changes in Young's modulus with the angle of the compressive strut with bed joint (□strut)

Experiments	Bed angle	□strut	E (Mpa)	E□□□□□
Prism compression experiment	0°	90°	6870	-
Horizontal loading test	0°	67.43°	5700	0.83
Diagonal compression experiment	49°	41°	1160	0.20

2.4.6 Comparison of results of Nepalese and Japanese historical brick masonry

Table 11 shows the comparison of G/E ratio for Nepalese and Japanese historical brick masonry. In the case of Nepalese historical brick masonry, the G/E ratio found was 16% (Mishra et al., 2020) while in Japanese historical brick masonry G/E ratio was 8%. The values of shear modulus are within the range of 8–16% of the value of modulus of elasticity E for Nepalese and Japanese historical brick masonry. In either case, the values of shear modulus were not close to 40% of E, as recommended by Eurocode 6. Tomaževič (2009) also reported that the actual values of G are within the range of 6–13% of the value of modulus of elasticity E. Experimental results of this study also collaborates with the findings of (Tomaževič, 2009).

Table 11: Comparison of G/E ratio for Nepalese and Japanese historical brick masonry

Brick masonry	Prism compression	Diagonal compression
Type of buildings	E (MPa)	G (MPa)
Nepalese	310	53
Japanese	6870	553

Where, G is the shear modulus and E is the modulus of elasticity

3 CONCLUSIONS

Numerical analysis was conducted on diagonal compression test and horizontal loading test models and following conclusions were made.

- The Poisson's ratio obtained from transducers gave closer analytical results to experimental results compared to Poisson's ratio obtained from Rosette's strain gauge.
- From the numerical analysis of diagonal compression model and from contours in the model, it was observed that most of the compressive forces pass through the centre of the specimen and are only concentrated in the area directly under the load rather than distributing to the whole cross-sectional area of the specimen.
- The highest value of the modulus of elasticity (E = 6870 MPa) was obtained for samples loaded perpendicularly to horizontal joints (θstrut=90°). For

the horizontal loading test, the value of E = 5700 MPa was obtained from the analysis (θstrut = 67.43°).

- The values of shear modulus G (calculated from the diagonal transducers in diagonal compression test) are within the range of 8–17% of the value of modulus of elasticity E (prism compression test) for Nepalese and Japanese historical brick masonry. Similar findings were reported by Tomaževič (2009). In either case, the values of shear modulus were not close to 40% of E, as recommended by Eurocode 6.

4 REFERENCES

[1] Abdulla, K. F., Cunningham, L. S., and Gillie, M. (2017). Simulating masonry wall behavior using a simplified micro-model approach. Engineering Structures, 151, 349-365.

[2] Annecchiarico, M., Portioli, F., and Landolfo, R. (2010). Micro and macro finite element modeling of brick masonry panels subject to lateral loadings. In Proc., COST C26 Action Final Conf (pp. 315-320).

[3] Dauda, J. A., Silva, L. C., Lourenço, P. B., & Iuorio, O. (2021). Out-of-plane loaded masonry walls retrofitted with oriented strand boards: Numerical analysis and influencing parameters. Engineering Structures, 243, 112683.

[4] Holler, S., Butenweg, C., Noh, S. Y., and Meskouris, K. (2004). Computational model of textile-reinforced concrete structures. Computers & structures, 82(23-26), 1971-1979.

[5] Hu, Y., Ma, P., and Yao, J. (2023). Effects of aspect ratios and vertical loads on in-plane seismic behavior of unreinforced masonry walls: A numerical simulation. Plos one, 18(3), e0282430.

[6] Kouris, L. A. S., and Triantafillou, T. C. (2018). State-of-the-art on strengthening of masonry structures with textile-reinforced mortar (TRM). Construction and Building Materials, 188, 1221-1233.

[7] Lourenço, P. B. (1998). Experimental and numerical issues in the modeling of the mechanical behavior of masonry.

[8] Ma, P., Yao, J., and Hu, Y. (2022). Numerical Analysis of Different Influencing Factors on the In-Plane Failure Mode of Unreinforced Masonry (URM) Structures. Buildings, 12(2), 183.

[9] Mishra, C., Yamaguchi, K., Endo, Y., Hanazato, T., & Shakya, M. (2020). Study on shear and flexural behavior of Nepalese masonry walls with and without reinforcement. In Proceedings of the 17th World Conference on Earthquake Engineering, Sendai, Japan (pp. 13-18).

[10] Mishra, C., Yamaguch, K., Araki, K., Ninakawa, T., and Hanazato, T. (2021). Structural behavior of brick wall specimens reinforced on the surface with RC walls under horizontal loading. Journal of Advanced Concrete Technology, 19(6), 593-613.

[11] Mishra, C., Yamaguchi, K., Araki, K., and Ninakawa, T. (2020). Diagonal compression test of the brick masonry reinforced on the surface with steel plates or RC walls. In Proc. 6th International Conference on Construction Materials, Fukuoka, Japan (pp. 27-29).

[12] Mishra, C., Yamaguchi, K., Jing, T., Hanazato, T., Endo, Y., and Shakya, M. (2023). Numerical Investigation of the Properties of Unreinforced and Reinforced Nepalese Historical Brick Masonry Structures. In International Conference on Structural Analysis of Historical Constructions (pp. 125-139). Cham: Springer Nature Switzerland.

[13] Mojsilović, N., Kostić, N., and Schwartz, J. (2013). Modeling of the behavior of seismically strengthened masonry walls subjected to cyclic in-plane shear. Engineering structures, 56, 1117-1129.

[14] Nowak, R., Kania, T., Derkach, V., Orłowicz, R., Halaliuk, A., Ekiert, E., and Jaworski, R. (2021). Strength parameters of clay brick walls with various directions of force. Materials, 14(21), 6461.

[15] Oliveira, L. M. F. D. (2014). Theoretical and experimental study of the behavior of vertical interfaces of interconnected structural masonry walls. (Doctoral dissertation, Universidade de São Paulo).

[16] Penna, A., Morandi, P., Rota, M., Manzini, C. F., Da Porto, F., and Magenes, G. (2014). Performance of masonry buildings during the Emilia 2012 earthquake. Bulletin of Earthquake Engineering, 12, 2255-2273.

[17] Roca, P., Cervera, M., Gariup, G., and Pela', L. (2010). Structural analysis of masonry historical constructions. Classical and advanced approaches. Archives of computational methods in engineering, 17, 299-325.

[18] Sun, A., Hou, S., and Lin, C. (2009). Failure mode analysis of buildings in Dujiangyan in Wenchuan earthquake. Journal of Dalian University of Technology, 49, 731-738.

[19] Standard, B. (2005). Eurocode 6-Design of masonry structures—. British Standard Institution. London, (2005).

[20] Tomaževič, M. (2009). Shear resistance of masonry walls and Eurocode 6: shear versus tensile strength of masonry. Materials and structures, 42, 889-907.